Acta Mechanica Solida Sinica
https://doi.org/10.1007/s10338-023-00423-x

Sound Reduction Control in Acoustic Enclosure with Air Ventilation

Mengyi Liu[1,2] · **Xiaoming Zhou**[1,2]

Received: 23 May 2023 / Revised: 8 August 2023 / Accepted: 9 August 2023

Abstract
An acoustic enclosure system with both interior sound reduction and air ventilation is designed and demonstrated. The system consists of a rectangular enclosed space coupled with ventilated metamaterials and microperforated panels (MPPs). By modeling the ventilated metamaterial as an impedance boundary condition, an analytic model is developed to characterize the frequency response of interior acoustic fields and evaluate the sound reduction performance of MPP structures. Numerical simulations are conducted to validate the accuracy of the theoretical model. It is found that the resonance response of the enclosure system can be suppressed by proper arrangement of the MPPs. Even with open area for airflow, the system still possesses good sound isolation originating from the low-transmission behavior of the ventilated metamaterial. The proposed model system may find potential applications in noise control engineering.

Keywords Acoustic enclosure · Sound reduction · Microperforated panel · Air ventilation

1 Introduction

Reducing the interior sound fields of acoustic enclosures is of vital importance in many industrial applications [1, 2], such as building rooms [3], ship cabins [4], and production workshops [5, 6]. In comparison with noise control in free-field scenarios, acoustic enclosure contains a finite volume; thus noise sources enclosed within the cavity induce sharp resonance peaks related to the normal modes of enclosures [7], making interior noises more difficult to suppress. Various models and strategies have been developed for sound reduction control in the enclosure system [8–12]. Microperforated panels (MPPs), firstly proposed by Maa [13], are widely used for interior sound attenuation. MPPs with the backing cavity behave as resonance-type acoustic absorbers and, when attached to the walls of enclosures, reduce interior sound intensity through energy dissipation. To accurately capture the interaction of MPPs with acoustic enclosures, Yang et al. [14] have stressed the importance of considering the compound structure MPPs as an integral part of the whole system, rather than just an absorption boundary condition.

Acoustic enclosures with ventilated openings allowing airflow are demanded in many circumstances, for example, in sound control of noisy machines with heat radiation. To this end, there is a need for the enclosure system capable of both sound attenuation and air ventilation. The advancement in metamaterial science has made it possible to create acoustic structures capable of both sound isolation and air ventilation [15–26]. However, sound control capabilities of ventilated metamaterials are usually evaluated in free-field situations, and the mechanisms of their application to acoustic enclosures are yet to be explored.

In this study, we extend the classical acoustic enclosure model by replacing the rigid walls with ventilated metamaterial barriers. By modeling open metamaterials as impedance boundary conditions, an analytical model is developed to characterize the frequency response of interior acoustic fields and evaluate the sound reduction performance of MPP-based absorbers. Numerical simulations for structured models are conducted to verify theoretical results. The proposed model can be used for the design of acoustic enclosures that require both noise reduction and air ventilation.

✉ Xiaoming Zhou
zhxming@bit.edu.cn

[1] Key Laboratory of Dynamics and Control of Flight Vehicle of Ministry of Education, Beijing Institute of Technology, Beijing 100081, China

[2] School of Aerospace Engineering, Beijing Institute of Technology, Beijing 100081, China

Published online: 28 August 2023

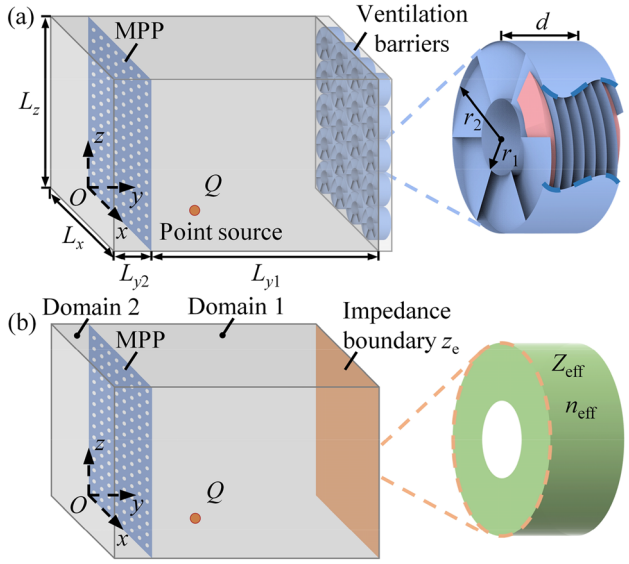

Fig. 1 **a** An acoustic enclosure system with the MPP structure for interior sound reduction and the open metamaterial structure for air ventilation; **b** an analytical model of the enclosure system where the metamaterial structure is modeled as an effective impedance boundary. Geometric parameters of the system are $L_{y1} = 60$ cm, $L_{y2} = 10$ cm, $L_x = 40$ cm, and $L_z = 50$ cm. The metamaterial structure has the thickness $d = 4.5$ cm, inner radius $r_1 = 2$ cm, outer radius $r_2 = 5$ cm, and helical pitch of 20 mm. The air has the mass density $\rho_0 = 1.21$ kg/m^3 and sound velocity $c_0 = 343$ m/s. The point source with the volume velocity $q = 2 \times 10^{-5}$ m^3/s locates at (4 cm, 6 cm, 5 cm)

2 Acoustic Enclosures with Ventilated Openings

2.1 Geometric Model

We begin with a classical acoustic enclosure model, which consists of a rectangular enclosed space with rigid walls, and is excited by an interior point source. The MPPs with the backing cavity are inserted within the enclosure for sound reduction purposes and are modeled in theory as part of the system instead of an absorptive boundary by following Yang's studies [14]. The rigid wall on the opposite side of the MPPs is replaced with an open acoustic metamaterial allowing airflow, which supports broadband sound isolation based on the Fano-like interference [18]. The entire enclosure system coupled with MPPs and open metamaterials is schematically shown in Fig. 1a.

The open metamaterial is a periodic structure of square lattices whose unit cell is made of six channels coiled up around a straight channel. The helical region can be homogenized with the effective refractive index n_{eff} and effective acoustic impedance Z_{eff} as shown in Fig. 1b. With the help of Green's function theorem, theoretical solutions for the coupling interaction between the helical region and straight channel can be obtained [18]. We further define an effective acoustic impedance for the ventilated metamaterial as

$$z_{\text{e}} = \frac{\overline{p}}{\overline{v}_n} \tag{1}$$

where $\overline{p}$ and $\overline{v}_n$ are, respectively, the averaging pressure and normal velocity over the input surface. Based on this effective-medium strategy, an analytical model can be established for the enclosure system based on the modal expansion method, as detailed in the next section.

2.2 Analytical Model

The system comprises the enclosure (domain 1) and the backing cavity of MPPs (domain 2), as described in Fig. 1b. Considering harmonic fields with time-dependence $e^{j\omega t}$, the Helmholtz equations in domain 1 and 2 are expressed, respectively, as

$$\nabla^2 p_1(\boldsymbol{r}) + k^2 p_1(\boldsymbol{r}) = -Q(\boldsymbol{r}) \tag{2}$$

$$\nabla^2 p_2(\boldsymbol{r}) + k^2 p_2(\boldsymbol{r}) = 0 \tag{3}$$

where p_i $(i = 1,2)$ denotes the acoustic pressure fields in the ith domain; $k = \omega/c_0$ with c_0 denoting the sound velocity; $Q(\boldsymbol{r}) = \text{j}\rho_0\omega q\delta(\boldsymbol{r}-\boldsymbol{r}_0)$ represents the point source located at $\boldsymbol{r}_0$ described by the Dirac delta function δ; ρ_0 and q are, respectively, the air density and volume velocity of the point source.

Based on the modal expansion method, the pressure fields in domains 1 and 2 can be expressed as

$$p_1(\boldsymbol{r}) = \sum_M A_M \phi_M(\boldsymbol{r}) \tag{4}$$

$$p_2(\boldsymbol{r}) = \sum_N B_N \varphi_N(\boldsymbol{r}) \tag{5}$$

where A_M is the Mth modal amplitude in domain 1; B_N is the Nth modal amplitude of domain 2; ϕ_M and φ_N denote the cavity modes of domains 1 and 2, respectively.

The boundary condition for surface impedance z_{e} can be expressed in terms of pressure p_1 as

$$\frac{\partial p_1}{\partial n} = -\text{j}\eta_{\text{e}} k p_1 \tag{6}$$

where the left-hand side denotes the pressure difference along the surface normal, and $\eta_{\text{e}} = \rho_0 c_0/z_{\text{e}}$ refers to the specific acoustic admittance. The boundary condition for the MPP surface (S_{MPP}) is expressed as

$$v_{n1} = \frac{p_1 - p_2}{z_{\text{MPP}}}, \quad v_{n2} = -v_{n1} \tag{7}$$

where $p_1 - p_2$ denotes the pressure difference across the MPP surface; v_{n1} and v_{n2} are the normal particle velocities in domains 1 and 2, respectively; z_{MPP} is the acoustic impedance of the MPP with the formula given by Maa [13].

According to the boundary condition (6), the acoustic modal fields of the Mth order in domain 1 can be generalized as

$$\phi_M(\boldsymbol{r}) = \cos\left(\frac{m\pi x}{L_x}\right)\cos\left(k_{yn}y\right)\cos\left(\frac{p\pi z}{L_z}\right) \tag{8}$$

where m and p denote the mode orders, and k_{yn} represents the nth root of k_y solved from the following eigenvalue equation

$$k_y \tan\left(k_y L_{y1}\right) = \mathrm{j}\eta_{\mathrm{e}} k \tag{9}$$

For the Mth-order mode with a specific set of m, n, and p, the eigenvalue of wave number for domain 1 is given by

$$k_M^2 = \left(\frac{m\pi}{L_x}\right)^2 + k_{ny}^2 + \left(\frac{p\pi}{L_z}\right)^2 \tag{10}$$

Similarly, the acoustic mode in domain 2 is expressed as

$$\varphi_N(\boldsymbol{r}) = \cos\left(\frac{m\pi x}{L_x}\right)\cos\left(\frac{n\pi}{L_{y2}}\left(y + L_{y2}\right)\right)\cos\left(\frac{p\pi z}{L_z}\right) \tag{11}$$

The system eigenvalue k_N of domain 2 is given by

$$k_N^2 = \left(\frac{m\pi}{L_x}\right)^2 + \left(\frac{n\pi}{L_{y2}}\right)^2 + \left(\frac{p\pi}{L_z}\right)^2 \tag{12}$$

To solve for the acoustic responses of the coupled system under a point source excitation, Green's theorem is applied to each domain, leading to

$$\begin{aligned}&\int_{\partial\Omega_1}\left(\phi_M(\boldsymbol{r})\frac{\partial p_1(\boldsymbol{r})}{\partial n} - p_1(\boldsymbol{r})\frac{\partial \phi_M(\boldsymbol{r})}{\partial n}\right)\mathrm{d}S\\ &= \int_{\Omega_1}\left(\phi_M(\boldsymbol{r})\nabla^2 p_1(\boldsymbol{r}) - p_1(\boldsymbol{r})\nabla^2\phi_M(\boldsymbol{r})\right)\mathrm{d}V\end{aligned} \tag{13}$$

for domain 1 occupying the space Ω_1 bordered by the surface $\partial\Omega_1$, and

$$\begin{aligned}&\int_{\partial\Omega_2}\left(\varphi_N(\boldsymbol{r})\frac{\partial p_2(\boldsymbol{r})}{\partial n} - p_2(\boldsymbol{r})\frac{\partial \varphi_N(\boldsymbol{r})}{\partial n}\right)\mathrm{d}S\\ &= \int_{\Omega_2}\left(\varphi_N(\boldsymbol{r})\nabla^2 p_2(\boldsymbol{r}) - p_2(\boldsymbol{r})\nabla^2\varphi_N(\boldsymbol{r})\right)\mathrm{d}V\end{aligned} \tag{14}$$

for domain 2 occupying the space Ω_2 with the boundary $\partial\Omega_2$.

With the help of Eqs. (2), (3), (6) and (7), Eqs. (13) and (14) are further written as

$$\begin{aligned}&\left(k_M^2 - k^2\right)\int_{\Omega_1}\phi_M(\boldsymbol{r})p_1(\boldsymbol{r})\mathrm{d}V\\ &+ \frac{\mathrm{j}\rho_0\omega}{z_{\mathrm{MPP}}}\int_{S_{\mathrm{MPP}}}\phi_M(\boldsymbol{r})(p_1(\boldsymbol{r}) - p_2(\boldsymbol{r}))\mathrm{d}S = \mathrm{j}\rho_0\omega q\phi_M(\boldsymbol{r}_0)\end{aligned} \tag{15}$$

$$\begin{aligned}&\left(k_N^2 - k^2\right)\int_{\Omega_2}\varphi_N(\boldsymbol{r})\,p_2(\boldsymbol{r})\,\mathrm{d}V\\ &+ \frac{\mathrm{j}\rho_0\omega}{z_{\mathrm{MPP}}}\int_{S_{\mathrm{MPP}}}\varphi_N(\boldsymbol{r})\,(p_2(\boldsymbol{r}) - p_1(\boldsymbol{r}))\,\mathrm{d}S = 0\end{aligned} \tag{16}$$

By substituting Eqs. (4) and (5) into Eqs. (15) and (16) and using the orthogonal property of modes, the equation system that governs the enclosure structure is given by

$$\begin{aligned}&\sum_{M'}A_{M'}\left[\left(k_M^2 - k^2\right)\Lambda^{(1)}_{M,M'} + \frac{\mathrm{j}\rho_0\omega}{z_{\mathrm{MPP}}}R^{(1)}_{M,M'}\right]\\ &- \frac{\mathrm{j}\rho_0\omega}{z_{\mathrm{MPP}}}\sum_N B_N C_{M,N} = \mathrm{j}\rho_0\omega q\phi_M(\boldsymbol{r}_0)\end{aligned} \tag{17}$$

$$\begin{aligned}&-\frac{\mathrm{j}\rho_0\omega}{z_{\mathrm{MPP}}}\sum_M A_M C_{M,N}\\ &+ \sum_{N'}B_{N'}\left[\left(k_N^2 - k^2\right)\Lambda^{(2)}_{N,N'} + \frac{\mathrm{j}\rho_0\omega}{z_{\mathrm{MPP}}}R^{(2)}_{N,N'}\right]\\ &= 0\end{aligned} \tag{18}$$

where we have defined

$$\begin{aligned}\Lambda^{(1)}_{M,M'} &= \int_{\Omega_1}\phi_M(\boldsymbol{r})\phi_{M'}(\boldsymbol{r})\mathrm{d}V\\ \Lambda^{(2)}_{N,N'} &= \int_{\Omega_2}\varphi_N(\boldsymbol{r})\varphi_{N'}(\boldsymbol{r})\mathrm{d}V\\ R^{(1)}_{M,M'} &= \int_{S_{\mathrm{MPP}}}\phi_M(\boldsymbol{r})\phi_{M'}(\boldsymbol{r})\mathrm{d}S\\ R^{(2)}_{N,N'} &= \int_{S_{\mathrm{MPP}}}\varphi_N(\boldsymbol{r})\varphi_{N'}(\boldsymbol{r})\mathrm{d}S\\ C_{M,N} &= \int_{S_{\mathrm{MPP}}}\phi_M(\boldsymbol{r})\varphi_N(\mathbf{r})\mathrm{d}S\end{aligned} \tag{19}$$

By setting the truncating numbers for M and N, modal amplitudes A_M and B_N can be solved by combining Eqs. (17) and (18). Eventually, the acoustic responses of the enclosure system can be evaluated based on Eqs. (4) and (5).

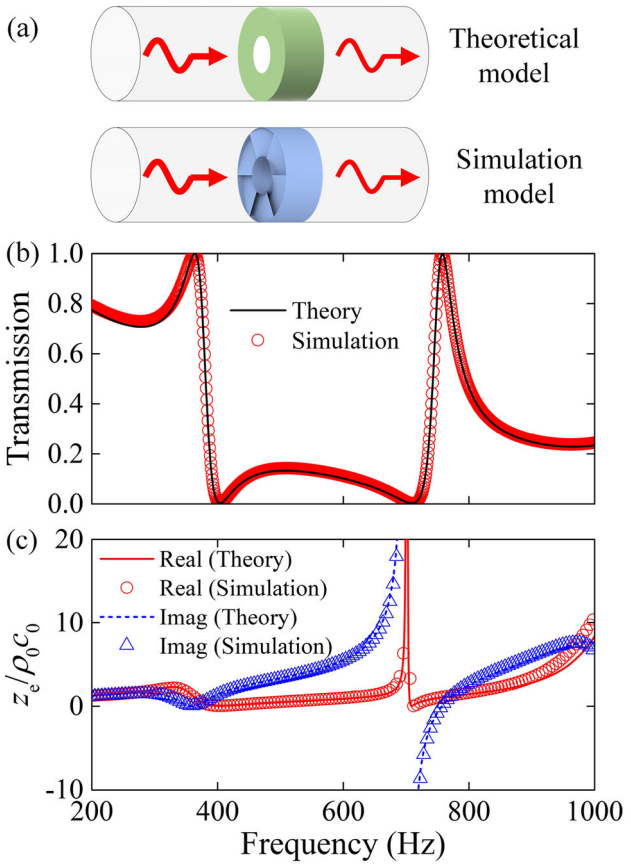

Fig. 2 **a** Schematic of theoretical and simulation models for the unit cell of the ventilated metamaterial; **b** acoustic transmission spectrum calculated by theoretical and simulation models; **c** effective acoustic impedance z_e at various frequencies

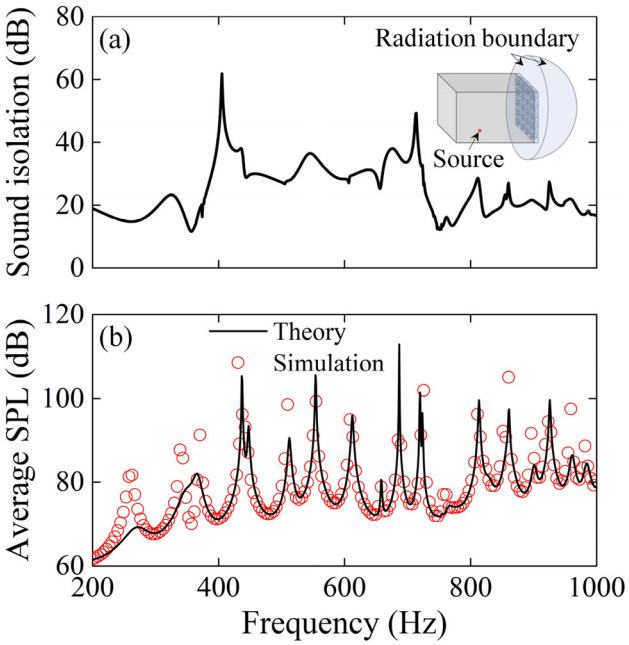

Fig. 3 Acoustic responses of the enclosure system without MPPs: **a** simulation results of the sound isolation; **b** average sound pressure level (SPL) of interior fields

3 Results and Discussions

3.1 Ventilated Enclosure without MPPs

For an open enclosure system, both interior fields and external sound leakage should be attenuated simultaneously. In the proposed system, the MPP structure is introduced to lower the interior pressure, while the ventilated metamaterial is used to block the sound leakage to the outside. In this section, we first consider the enclosure system without MPPs to evaluate the sound isolation effect of ventilated metamaterials.

Consider the unit cell structure as illustrated in Fig. 2a. Figures 2b and c show the acoustic transmission spectrum and effective impedance z_e of ventilated metamaterials, respectively. Excellent agreement between the theoretical and simulation results can be found. In Fig. 2b, the transmission drops significantly in the frequency range from 400 to 700 Hz because of the Fano-like interference [18]. This defines the range of working frequency for the enclosure system to prevent sound leakage. For verification, numerical simulation is performed for the enclosure system equipped with the ventilated metamaterial. To calculate the sound leakage, a semi-spherical domain bordered with the radiation boundary condition is added to the output side of the ventilated barrier. The isolation performance can be evaluated by examining the difference in sound pressures between the interior and external regions of the system. To this end, we define the sound isolation (SI) as

$$\mathrm{SI} = 10\log\left(\int_{\Omega}|p|^2/V\,\mathrm{d}v \Big/ \int_{S_\mathrm{R}}|p|^2/S\,\mathrm{d}s\right) \tag{20}$$

where V refers to the volume of the enclosure system (Ω), and S denotes the surface area of the radiation boundary (S_R). As shown in Fig. 3a, the sound isolation exceeds 20 dB at frequencies from 400 to 700 Hz, corresponding well to the low-transmission band in Fig. 2b. These results clearly demonstrate the good isolation effect of the ventilated metamaterial.

Next, let's analyze the frequency response of the interior sound fields. By using the impedance results z_e as given in Fig. 2c, we can calculate the interior sound fields within the enclosure according to the analytical model developed in Sect. 2.2. Figure 3b shows the sound pressure level (SPL) averaged over the enclosed space. Here, the average SPL is defined as [27]

$$\mathrm{SPL} = 10\log\left(\left\langle p_\mathrm{e}^2\right\rangle/p_\mathrm{ref}^2\right),\ \text{with}\ \left\langle p_\mathrm{e}^2\right\rangle = \int_{\Omega}|p|^2\mathrm{d}v/(2V) \tag{21}$$

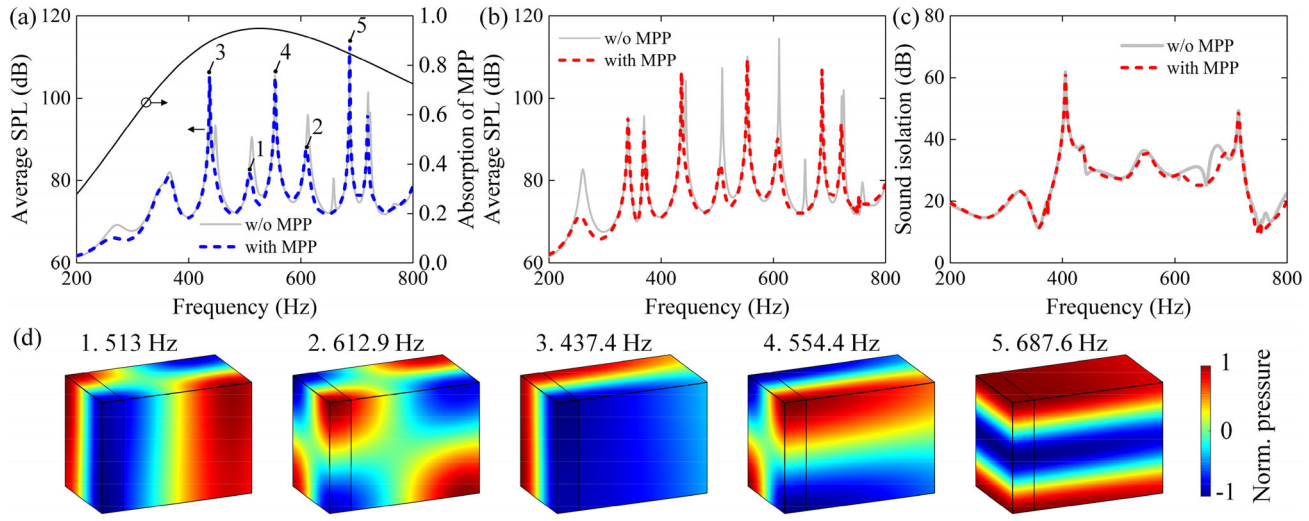

Fig. 4 **a** Theoretical results of average SPL of the enclosures with and without the MPP structure, and acoustic absorption coefficient of the MPP with a backing cavity of $L_{y2} = 10$ cm; **b** simulation results of average SPL of the enclosure system; **c** sound isolation of the enclosures with and without the MPP structure; **d** acoustic pressure distributions at frequencies of 513 Hz, 612.9 Hz, 437.4 Hz, 554.4 Hz, and 687.6 Hz corresponding to different resonance peaks in **a**

where $p_{\text{ref}} = 2 \times 10^{-5}$ Pa is the reference sound pressure. In barrier frequencies from 400 to 700 Hz, good agreement between the analytical and numerical results can be found, validating the theoretical model. As a typical feature of the enclosure system, sharp resonant peaks appear in this frequency range. MPPs with the backing cavity will be employed to suppress these resonant responses, as presented in the next section.

3.2 Sound Reduction Control in Enclosures with MPPs

The MPP with the cylindrical pore is employed, of which the depth, diameter, and perforation ratio are 0.35 mm, 0.35 mm, and 0.01, respectively. The dynamic viscosity of air in the micro holes is set as 1.85×10^{-5} Pa·s [13]. The good absorption performance of MPP and its working frequency are associated with the configuration of the backing cavity. We first consider the case of a rectangular cavity. Figure 4a shows the sound absorption spectrum of MPPs with a backing cavity of depth $L_{y2} = 10$ cm in the normally incident case. Here, the cavity size is chosen such that the working band of absorptive MPPs is consistent with the barrier frequency of the ventilated metamaterial.

Figures 4a and b show, respectively, the theoretical and simulation results of the average SPL for the enclosure systems with and without MPPs, and good agreement can be observed between them. Partial resonance peaks have been damped by the MPP structure. To understand the underlying mechanism, acoustic pressure field distributions are provided in Fig. 4d for the damped peaks at 513 Hz and 612.9 Hz, and for the undamped peaks at 437.4 Hz, 554.4 Hz, and 687.6 Hz. MPPs are known to operate when there is an evident pressure phase contrast on both sides in order to induce effective air motion within the micro holes. This explains the good damping effect at the two damped peaks. For the undamped peaks, the MPP is not activated because of the in-phase distribution of acoustic pressure across the MPP surface. Figure 4c shows the sound isolation spectrum of the enclosure with the MPP structure. The isolation performance is guaranteed by the large transmission loss of the ventilated metamaterial, so the good isolation effect can still be observed.

To cope with the remaining undamped peaks, the MPP is placed in an unparallel manner. We first postulate a configuration where the backing cavity of the MPP is divided into two prisms with the triangular cross section, as shown in Fig. 5a. The average SPL inside the enclosure is shown in Fig. 5b. The resonance peaks at 437.4 Hz and 554.4 Hz have been damped except for the one at 687.6 Hz. To gain a deeper insight into the performance, acoustic pressure distributions are plotted in Fig. 5c. For the damped case, the evident pressure contrast on both sides of the MPP can be seen, which activates the MPP to absorb sounds. The resonance at frequency 687.6 Hz cannot be damped because the wave patterns on both sides of the MPP still remain the same. To further enhance the damping effect, a rather complex configuration is considered, as shown in Fig. 6a, where the backing cavity is composed of four rectangular pyramids. The average SPL of this model system is shown in Fig. 6b. The resonance peak at 687.6 Hz has been removed because of the enhanced pressure contrast across the MPP as seen from the field pattern in Fig. 6c. Figures 5d and 6d present the sound isolation spectra of the two enclosure systems. The isolation performance depends primarily on the transmission

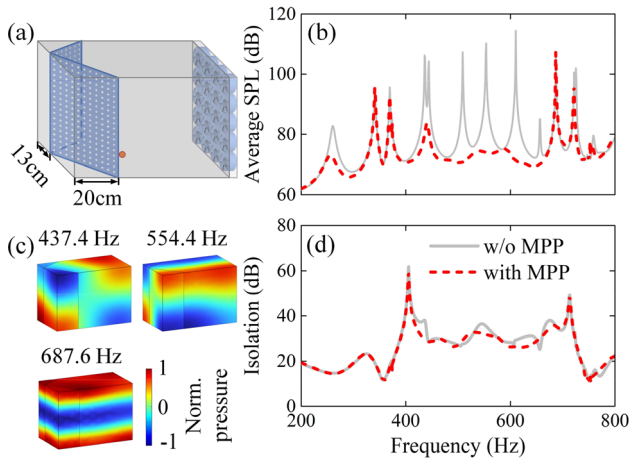

Fig. 5 **a** Acoustic enclosure systems in which the backing cavity of the MPP is composed of two prisms with the triangular cross section; **b** average SPL of the enclosure system; **c** acoustic pressure distributions at different frequencies; **d** sound isolation of the enclosure system

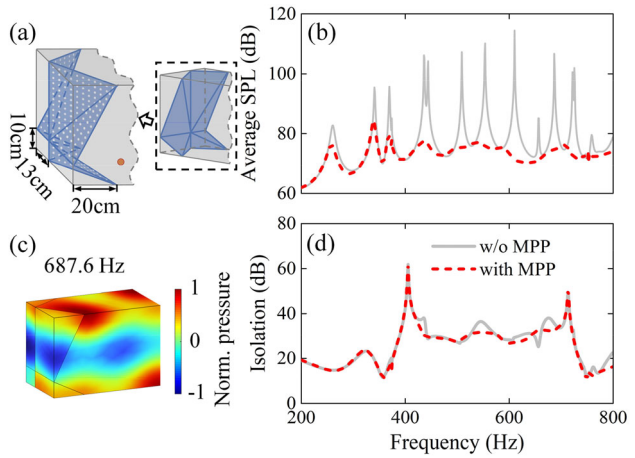

Fig. 6 **a** Acoustic enclosure systems in which the backing cavity of the MPP is composed of four rectangular pyramids; **b** average SPL of the enclosure system; **c** acoustic pressure distribution at frequency 687.6 Hz; **d** sound isolation of the enclosure system

of sounds across the metamaterial. Although the MPP configurations are changed, the metamaterial structure remains the same. Thereby, the good sound isolation is preserved and not affected by the MPP structures.

4 Conclusion

This paper presents an extension of the study on acoustic enclosure systems by replacing a rigid wall with the ventilated acoustic metamaterial. By modeling open metamaterials as impedance boundary conditions, an analytical acoustic model is developed for the ventilated enclosure system based on the modal expansion method. The accuracy of the analytical model is demonstrated by numerical simulations. The interior sound reduction of enclosure systems based on MPPs with backing cavities is studied. It is found that the resonance response of the enclosure system can be suppressed by the proper arrangement of MPPs. The open barrier exhibits good sound isolation originating from the low-transmission behavior of the ventilated metamaterial. As a result, an acoustic enclosure system capable of both interior sound reduction and air ventilation is realized, which is expected to find potential applications in noise control engineering.

Author contributions ML and XZ conceived the concept and model. ML carried out the theoretical analyses and numerical simulations. XZ supervised the research. Both authors discussed the results and wrote the manuscript.

Funding This work was supported by the National Natural Science Foundation of China (Grant Nos. 12225203, 11622215, and 11872111) and the 111 Project (Grant No. B16003).

Availability of Data and Material The data that support the findings of this study are available from the corresponding author upon reasonable request.

Declarations

Conflict of interest The authors declare that they have no competing interests.

References

1. Eleftheriou PC. Industrial noise and its effects on human hearing. Appl Acoust. 2002;63(1):35–42.
2. Lie A, Skogstad M, Johannessen HA, Tynes T, Mehlum IS, Nordby KC, et al. Occupational noise exposure and hearing: a systematic review. Int Arch Occup Environ Health. 2016;89(3):351–72.
3. Beristain S. Machinery noise in a commercial building. J Acoust Soc Am. 2017;141(5):3685–3685.
4. Bouzón R, Costa AM, Roshan G, Orosa JA. Evaluating the consequences of the new standards on noise conditions in ships. Pollution. 2015;1(2):127–38.
5. Bley H, Günther KG, Haeusler J, Noé EL, Rosenkranz W. Machine concentration and noise annoyance in the workshop. CIRP Ann. 1980;29(1):269–73.
6. Saraei M, Omidi R, Aminian O, Izadi N, Akbarpour S, Ebrahimi MS. The combined effect of noise and solvent exposure on hearing loss in the tire factory workers. Indian J Otolaryngol Head Neck Surg. 2022;74(3):3887–92.
7. Kuttruff H. Room acoustics. London: CRC Press; 2016.
8. Morse PM, Bolt RH. Sound waves in rooms. Rev Mod Phys. 1944;16(2):69–150.
9. Dowell EH, Gorman GF, Smith DA. Acoustoelasticity: General theory, acoustic natural modes and forced response to sinusoidal excitation, including comparisons with experiment. J Sound Vib. 1977;52(4):519–42.
10. Kubota Y, Dowell EH. Asymptotic modal analysis for sound fields of a reverberant chamber. J Acoust Soc Am. 1992;92(2):1106–12.

11. Kopuz S, Lalor N. Analysis of interior acoustic fields using the finite element method and the boundary element method. Appl Acoust. 1995;45(3):193–210.
12. Xu B, Sommerfeldt SD. A hybrid modal analysis for enclosed sound fields. J Acoust Soc Am. 2010;128(5):2857–67.
13. Maa DY. Theory and design of microperforated panel sound-absorbing constructions. Sci Sin. 1975;18(1):55–71.
14. Yang C, Cheng L. Sound absorption of microperforated panels inside compact acoustic enclosures. J Sound Vib. 2016;360:140–55.
15. Cheng Y, Zhou C, Yuan BG, Wu DJ, Wei Q, Liu XJ. Ultra-sparse metasurface for high reflection of low-frequency sound based on artificial Mie resonances. Nat Mater. 2015;14(10):1013–9.
16. Zhang HL, Zhu YF, Liang B, Yang J, Yang J, Cheng JC. Omnidirectional ventilated acoustic barrier. Appl Phys Lett. 2017;111(20):203502.
17. Wu X, Au-Yeung KY, Li X, Roberts RC, Tian J, Hu C, et al. High-efficiency ventilated metamaterial absorber at low frequency. Appl Phys Lett. 2018;112(10):103505.
18. Ghaffarivardavagh R, Nikolajczyk J, Anderson S, Zhang X. Ultra-open acoustic metamaterial silencer based on Fano-like interference. Phys Rev B. 2019;99(2):024302.
19. Kumar S, Xiang TB, Lee HP. Ventilated acoustic metamaterial window panels for simultaneous noise shielding and air circulation. Appl Acoust. 2020;159:107088.
20. Chen DC, Wei Q, Yan PY, Zhu XF, Wu DJ. Sound insulation via a reconfigurable ventilation barrier with ultra-thin zigzag structures. J Appl Phys. 2021;129(6):064502.
21. Dong R, Mao D, Wang X, Li Y. Ultrabroadband acoustic ventilation barriers via hybrid-functional metasurfaces. Phys Rev Appl. 2021;15(2):024044.
22. Dong R, Mao D, Zhu Y, Mo F, Wang X, Li Y. A ventilating acoustic barrier for attenuating broadband diffuse sound. Appl Phys Lett. 2021;119(26):263505.
23. Nguyen HQ, Wu Q, Chen H, Chen JJ, Yu YK, Tracy S, et al. A Fano-based acoustic metamaterial for ultra-broadband sound barriers. Proc Royal Soc A. 2021;477(2248):20210024.
24. Xiao Z, Gao P, Wang D, He X, Wu L. Ventilated metamaterials for broadband sound insulation and tunable transmission at low frequency. Extreme Mech Lett. 2021;46:101348.
25. He J, Zhou Z, Zhang C, Zheng Y, Li Y, Li Y, et al. Ultrasparse and omnidirectional acoustic ventilated meta-barrier. Appl Phys Lett. 2022;120(19):191701.
26. Zhang R, Wang G, Zhou X, Hu G. A decoupling-design strategy for high sound absorption in subwavelength structures with air ventilation. JASA Express Lett. 2022;2(3):033602.
27. Cheng L, Nicolas J. Radiation of sound into a cylindrical enclosure from a point-driven end plate with general boundary conditions. J Acoust Soc Am. 1992;91(3):1504–13.